A Braided Skeleton Surgical Manipulator with Tunable Diameter *

Conference Paper · November 2020

DOI: 10.1109/BioRob49111.2020.9224312

4 authors, including:

Zufeng Shang
Zhejiang Sci-Tech University
13 PUBLICATIONS **33** CITATIONS
SEE PROFILE

Jiayao Ma
University of Oxford
67 PUBLICATIONS **1,049** CITATIONS
SEE PROFILE

Shuxin Wang
Xiamen University
183 PUBLICATIONS **3,167** CITATIONS
SEE PROFILE

2020 8th IEEE International Conference on Biomedical
Robotics and Biomechatronics (BioRob)
New York, USA. Nov 29 - Dec 1, 2020

A Braided Skeleton Surgical Manipulator with Tunable Diameter *

Zufeng Shang, Jiayao Ma, Zhong You, and Shuxin Wang

Abstract— **In natural orifice transluminal endoscopic surgery (NOTES), the manipulator design is a great challenge because it needs to meet different requirements for stiffness and size during the whole process. In our recent work, a braid-based manipulator has been proposed, which behaves as a stand-alone braid to fold and deploy in normal state, but turns to be rigid when a negative pressure is applied. It exhibits a stiffness ratio of 6.85 and diameter variability, but the control of the tunable diameter was not declared. In this paper, a bi-directional tunable-diameter mechanism for the braided skeleton is proposed, which uses shape memory alloy (SMA) braided fibers to deploy to a large profile state by electric heating, and rubber bands to force the skeleton back to the slim state when cooled. The mechanism is validated with a physical model, which can achieve a ratio of 1.46 between the maximum and minimum diameters. A theoretical model is also established based on the open-coiled theory, and parametric analysis is conducted to further detail the mechanism. The results show the promise of the mechanism in braided manipulator.**

I. Introduction

The natural orifice transluminal endoscopic surgery (NOTES) explains a new surgical procedure during which the tools are inserted into body cavity via body orifices [1]. It has advantages including smaller scars, less postoperative pain, shorter hospitalization, and earlier rehabilitation [2-4], and has been regarded as the future tendency of surgical operation since it appeared [5, 6]. Fortunately, NOTES is finding its way from lab experiments to clinical trials [7]. A NOTES can be a transvaginal, transgastric or transcolonic process [7]. No matter which route is selected, the passageway is narrow and tortuous, making it difficult to insert the device unless it is slim and flexible [8, 9]. However, a multifunctional device should have channels for surgical tools, light, water, and image [10], making it difficult to reduce the overall size. In addition, the device should be flexible during insertion [8] whereas exhibit enough stiffness to guarantee enough force capability during operation [9]. As a result, the different requirements for stiffness and size make the manipulator design challenging.

* This work was supported by the National Key R&D Program of China (Grant No. 2017YFC0110401) and the National Natural Science Foundation of China (Grant 51520105006 and Grant 51721003).

Zufeng Shang is with the Key Laboratory of Mechanism Theory and Equipment Design of Ministry of Education, Tianjin University, Tianjin, 300350 China. (e-mail: szf_rai@tju.edu.cn).

Jiayao Ma is with the Key Laboratory of Mechanism Theory and Equipment Design of Ministry of Education, Tianjin University, Tianjin, 300350 China. (corresponding author to provide phone: +86-22-85356291; fax: +86-22-85356291; e-mail: jiayao.ma@tju.edu.cn).

Zhong You is with the Department of Engineering Science, University of Oxford, Oxford, OX1 3PJ, UK. (e-mail: zhong.you@eng.ox.au.ck).

Shuxin Wang is with the Key Laboratory of Mechanism Theory and Equipment Design of Ministry of Education, Tianjin University, Tianjin, 300350 China. (corresponding author to provide phone: +86-22-87402173; fax: +86-22-87402173; e-mail: shuxinw@tju.edu.cn).

As for the conflict in stiffness, a tubular manipulator with tunable stiffness can be a solution [8, 10]. In our previous work [11], a braided manipulator has been proposed. It takes a braided tube as skeleton and wears the membrane as sealing cover. When the cavity is vacuumed, the manipulator turns to be rigid as the air pressure compressing the membrane to the skeleton. It experimentally exhibits a bending stiffness ratio of 6.9 between rigid and flexible states. Like other tunable stiffness mechanisms using vacuum, such as Layer Jamming [12], Dragon skin [13], Slider Linkage [14] and Stiff-Flop [15], it is very safe and responses in seconds, which are vital in surgery. In addition, what makes the braided manipulator distinct is the tunable diameter, i.e., the manipulator functions as a stand-alone braid for the membrane and the braid are separated without negative pressure [11]. In this state, it can deploy and fold under external load to achieve the tunable diameter [16, 17], thereby showing promise in solving conflicts not only in stiffness but also in size.

Despite that the braided manipulator is promising, no practical category to control the diameter has been proposed. By contrast, in the field of stenting, there are basically two common-used methods to deploy a braided stent for restoring the blood flow [18, 19]. One is known as self-expandable stent which is fabricated with nitinol. With the superelasticity, it can deploy automatically when released from a thin guide tube [20, 21]. The other is using a balloon inflated inside the stent to achieve deployment [19]. The stents are supposed to be left in the blood vessels forever, and the methods are both for deploying the stent with no folding and withdrawing. As a result, both methods are not applicable to the braided manipulator.

In this paper, we focus on the braided skeleton of the manipulator and propose a method to achieve the bi-directional tunable diameter of the braided manipulator. It adopts shape memory alloy (SMA) fibers to deploy and rubber bands to fold. This paper is organized as follows. In Section II, the mechanism of the tunable diameter and the prototype fabrication process are detailedly introduced. In Section III, an analytical model is established to explain the mechanism. Section IV introduces the experimental setup, followed by results and discussions in Section V. Conclusion is given in Section VI which ends this paper.

II. Method and Materials

A. Tunable Diameter Mechanism

The tunable diameter mechanism of the braided tube is shown in Fig. 1. The braided skeleton is composed of SMA fibers, tubular coats and rubber bands. The SMA fibers are one-way shape memorized, which can reshape themselves to be helixes with a large diameter when heated to its transition temperature. Following the helical configuration, it is easy to manually braid the fibers on a mould [22], and the final diameter of the obtained braided structure will be the same as

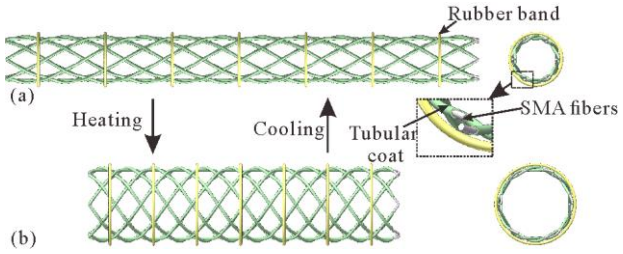

Figure 1. Tunable diameter mechanism: (a) small profile and (b) large profile

that of the mould. The electric heating method is adopted, and a tubular coat is covered on each fiber for electricity insulation. Elastic rubber bands are dressed on the outer surface of the braided tube. The bands are small circles and are tensioned on the tube. The SMA fibers are flexible at room temperature, thus the bands are strong enough to fold the tube, as shown in Fig. 1(a). When heating is applied, the braided tube expands radially, turning to the large pre-configured profile. In addition, the fibers are rigid at a higher temperature, making the whole structure rigid enough to sustain the bands and exhibit a larger profile, as shown in Fig. 1(b). When heating is cancelled, the fibers are easily deformed again as the temperature drops. As a result, the whole structure recovers to the slim state under the stressed rubber bands.

B. Materials and Fabrication

There are three major fabrication steps for the skeleton. The first step is to design the shape memory effect. Nitinol fiber is selected as the shape memory material for its substantial moduli difference between austenitic and martensitic phases [23]. The fibers are fixed in the helical grooves of a steel rod. After a heat treatment at 480°C for one hour and cooling at room temperature, the fibers are helical-shaped and obtain one-way shape memory at a transition temperature of 55°C. The second is to obtain the braided fibers. To provide enough strength, double-braid configuration is adopted and two fibers constitute one group. The two fibers are then inserted into a Teflon tube, which serves as a coat for electricity insulation. Third, a braided tube is acquired by braiding twelve fibers on a 3D-printed mould [22]. The mould, the helical fibers, and the final braided tube share the same helical parameters. Thus, the braiding process is coordinated and the fibers in the braided tube keep their original configuration. The length, the outer diameter and the braiding angle of the final braided tube in the sufficiently heated state are 144.8mm, 26.0mm and 47.8°, respectively.

TABLE I. PARAMETERS OF THE PHYSICAL MODEL

Parameters	Values
Length L	144.8mm
Diameter D_{outer}	26.0mm
Fiber number n	12*2
Braiding angle β	47.8°
Nitinol Fiber diameter d	0.5mm
Fiber Young's modulus E	41.56Gpa (at I=2A)
	7.76Gpa (at I=0A)
Tubular coat outer diameter d_c	1.6mm
Rubber band length c	32mm
Rubber band elasticity E_w	0.77N
Number of the rubber bands m	4
Density of the rubber band distribution L/m	36.2mm

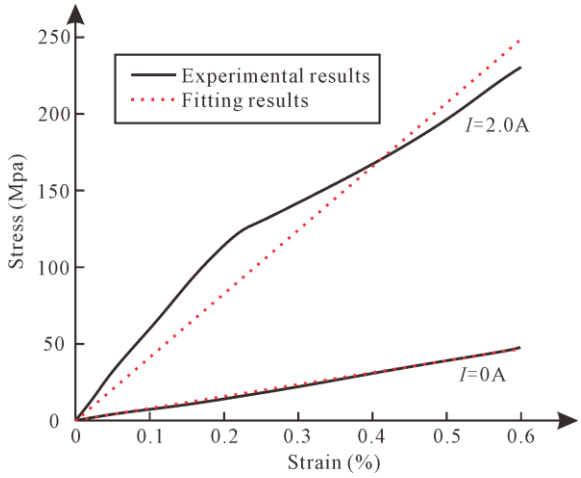

Figure 2. Stress-strain curves of the nitinol fibers at different electric currents

The Young's modulus of the fibers at different electric currents is determined through tensile test, which is conducted on an Instron 5982 testing machine, following ASTM F2516-14. Numerical result based on the Abaqus shows that the maximum strain of the braided fibers during the diameter changing process is 0.6%. Thus, the stress in the strain range of 0-0.6% is considered and the stress versus strain curves are presented in Fig. 2. It can be seen that the curves at lower electric currents (0A and 0.5A) are perfectly linear and those at higher electric currents (1 A and 2A) slow down slightly but never reach a plateau. Here, the material is regarded as linearly elastic, and the Young's modulus is calculated with the experimental results and listed in Tab. I.

Electric heating method is adopted to simplify the control system, and a new configuration of the braided tube is designed. As shown in Fig. 3, the fiber ends are connected one by one with electric wires: a dextral fiber is connected to a sinistral one. As a result, all fibers form an only-one circuit, controlled by a power supply. Connections between the fibers and the wires are fastened with compression, and thus have a good strength. Rubber tube is coated at the joint for insulation. In addition, the rubber bands are uniformly distributed on the outer surface of the tube, obtaining the final physical model. All parameters are listed in Tab. I.

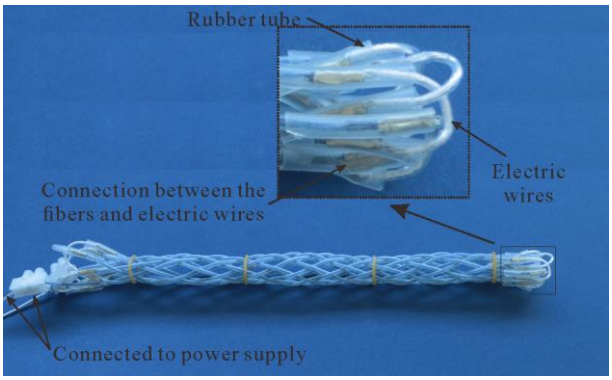

Figure 3. Physical model of the braided tube with tunable diameter

III. THEORETICAL MODEL: DIAMETER RANGE

Nitinol outstands for its phase change between austenite and martensite, which makes it exhibit the greatly different Young's modulus. The phase change process is complicated despite that many theoretical models have been proposed. What's more, here the theoretical model doesn't focus on the dynamic results but only concerns the final diameter range. Therefore, to simplify the problem, the heat transmission process is ignored, and the braided tube is assumed to be cooled down instantly. In addition, the effect of the Teflon cover is not included.

With the above assumptions, the tunable diameter mechanism can be explained with Fig. 4. Fig. 4(a) presents the fully deployed braided tube with a diameter of D_1. It is heated and the fibers have a Young's modulus of E_1. As in the case of the skeleton of the manipulator as shown in Fig. 4(b), the rubber bands are covered on the outer surface, which compress the tube from its original diameter D_1 to the largest diameter D_2 of the manipulator. When heating is stopped, the tube cools down and the Young's modulus decreases to E_2. At this circumstance, the cooled tube obtains its stress-free diameter D_2, and is forced to be slimmer compressed by the rubber bands. Finally, the diameter reaches the bottom of the range, the smallest diameter, D_3. Therefore, D_1 is determined by the heat treatment process during the fabrication, whereas D_2 and D_3 are determined by the relationship between the stiffness of the braided tube and the load caused by the rubber bands.

Next, equations for the relationships between the radial load and the diameter of both the braided tube and the bands are focused. The equation for the braided tube is given by Jedwab and Clerc [24] as follows:

$$\begin{cases} P_{\mathrm{b}} = \dfrac{4n\cos^2\beta_0}{\pi {D_0}^2 \sin^2\beta} \times \\ \left[\dfrac{2GI\cos\beta}{K_3}\left(\dfrac{2\sin\beta}{K_3} - K_1\right) - \dfrac{EI\tan\beta}{K_3}\left(\dfrac{2\cos\beta}{K_3} - K_2\right)\right] \\ D_{\mathrm{b}} = D_0\cos\beta / \cos\beta_0 \end{cases} \quad (1)$$

where

$K_1 = \sin 2\beta_0 / D_0$, $K_2 = 2\cos^2\beta_0 / D_0$, $K_3 = D_0 / \cos\beta_0$, P_{b} and D_{b} are respectively the radial pressure and diameter of the tube, and original parameters are denoted with footmark "$_0$". Thus, the relationship between P_{b} and D_{b} can be determined at a given original configuration of D_0, β_0 and E, and expressed as $P_{\mathrm{b}} \sim D_{\mathrm{b}}(D_0, \beta_0, E)$. As for the radial compression pressure of the rubber bands, based on the material mechanics, it can be calculated as

$$P_{\mathrm{r}} = \frac{2mE_{\mathrm{w}}(D_{\mathrm{r}} / D_0 - 1)}{D_{\mathrm{r}} L} \quad (2)$$

and expressed as $P_{\mathrm{r}} \sim D_{\mathrm{r}}(D_0, E_{\mathrm{w}})$. In the equation, P_{r} and D_{r} are respectively the radial pressure and diameter of the bands. The bands are covered on the outer surface of the braided tube, so we can also have following equations

$$P_{\mathrm{b}} = P_{\mathrm{r}} \quad (3)$$

$$D_{\mathrm{b}} = D_{\mathrm{r}} - 2d_{\mathrm{c}} \quad (4)$$

Solving the four unknown variables including P_{b}, P_{r}, D_{b} and D_{r} with Eqs. (1-4), the final diameter can be determined at a given original configuration including diameter, braiding angle and Young's modulus of the fibers and the bands. Therefore, the largest and the smallest diameters can be calculated as $D_2(D_1, \beta_1, E_1, E_{\mathrm{w}})$ and $D_3(D_2, \beta_2, E_2, E_{\mathrm{w}})$, respectively.

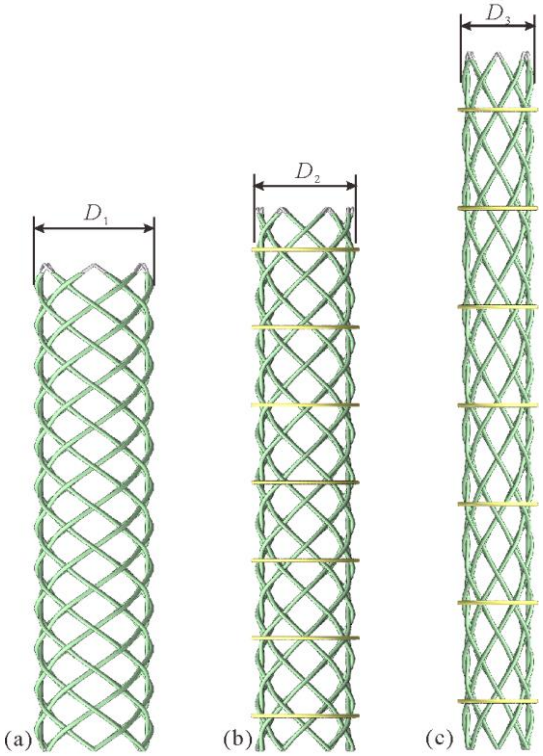

Figure 4. Diameters of the (a) fully deployed braided tube, (b) deployed skeleton and (c) folded skeleton

IV. EXPERIMENTAL SETUP

A. Tunable Diameter

The nitinol braided tube is heated with a power supply which can provide constant current, as shown in Fig. 5. All fibers can be charged at the same time. When the temperature of the structure gets to be stable, the phase change process is completed, and the shape of the braided tube is fixed. The outer diameter is recorded as the maximum diameter and then the heating is stopped. The tube is left in the room temperature to be gradually cooled. When it returns to the slim configuration, the outer diameter is recorded as the minimum diameter.

B. Response Time

The response time is determined based on Young's modulus of the nitinol varying with temperature. The overall stiffness of the tube varies during the phase change and gets to

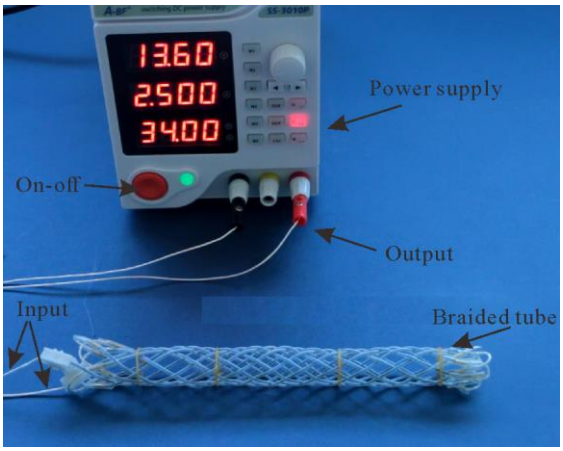

Figure 5. Experimental setup for the tunable diameter

be stable when the phase change is completed. To detect the overall stiffness change, cantilever test condition is established and the force versus displacement curve is focused on. One end of the skeleton is fixed and the other is forced downwards with a force sensor, which moves with a constant speed of 10mm/min. The braided tube is charged during the load process and the stiffness change is observed.

V. Results and Discussions

A. Diameter Range

The diameter range in the experiment is shown in Fig. 6. Fig. 6(a) presents the skeleton heated by the electric current of 2.0A, which has an average diameter of 21.4mm. When cooled down, it recovers to the slim state shown in Fig. 6(b), whose diameter is 14.7mm.

The theoretical results are presented in Fig. 7. In the figure, the pressure versus diameter curves of the rubber band and the heated tube meet at point *A*, forming a stable diameter of

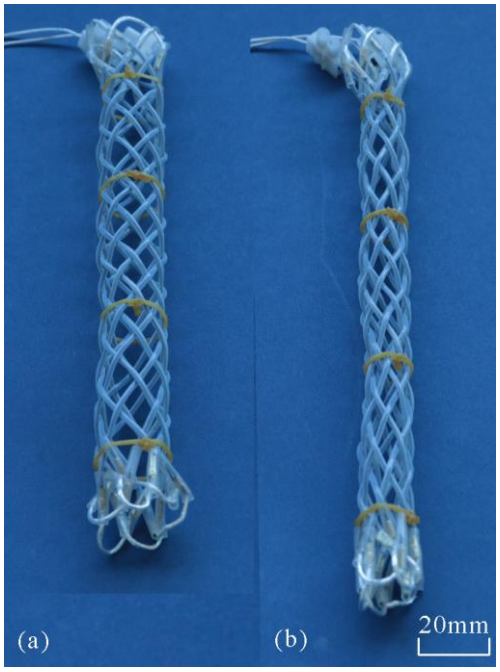

Figure 6. Experimental (a) maximum diameter and (b) minimum diameter

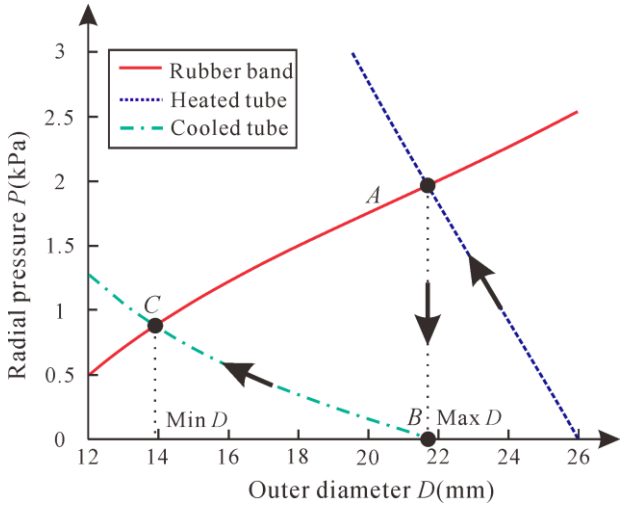

Figure 7. Theoretical relationships between the outer diameter and the radial load of the band and tubes

21.7mm, i.e., the maximum diameter. With the assumption that the phase change process is completed instantly, it changes from point *A* to point *B*, which share the same geometrical parameters. Then, the diameter decreases to the point *C* following the curve of the cooled tube, where curves of the cooled tube and the rubber band meet. The minimum diameter is 13.9mm. Tab. II lists the errors between the theoretical and the experimental results for maximum and minimum diameters, which are respectively 1.40% and 5.44%, validating the theoretical model.

With the theoretical model, parametric analysis is conducted to analyze the effects of rubber bands on the tunable diameter of the skeleton. The concerned parameters include the elasticity, the distribution, and the circumference of the rubber bands, and the results are presented in Fig. 8. It can be seen in Fig. 8(a) that both the maximum and the minimum diameters decrease with the elasticity of the rubber bands. However, the diameter range is not monotone and with a maximum at the elasticity of around 0.6 N/ε. With weak bands, the compression is too limited to force the cooled tube to be compacted. In contrast, if the bands are too strong, the heated tube will have difficulty in resisting the large compression. Therefore, the elasticity of the band should be moderate. Fig. 8(b) analyzes the varied distribution, with different average length of the tube for per band. A higher distribution means fewer rubber bands. Because both distribution and elasticity directly affect the compression with the same mechanism, the effects of the distribution are similar as the elasticity. The distribution shouldn't be too large nor too small. Fig. 8(c) shows variation of the diameters with the circumference. It can be seen that the diameter range is higher at a smaller band circumference. At a smaller circumference,

TABLE II. Results of the Diameter Range

Diameter	Experimental value	Theoretical value	Error
Maximum	21.4mm	21.7mm	1.40%
Minimum	14.7mm	13.9mm	5.44%

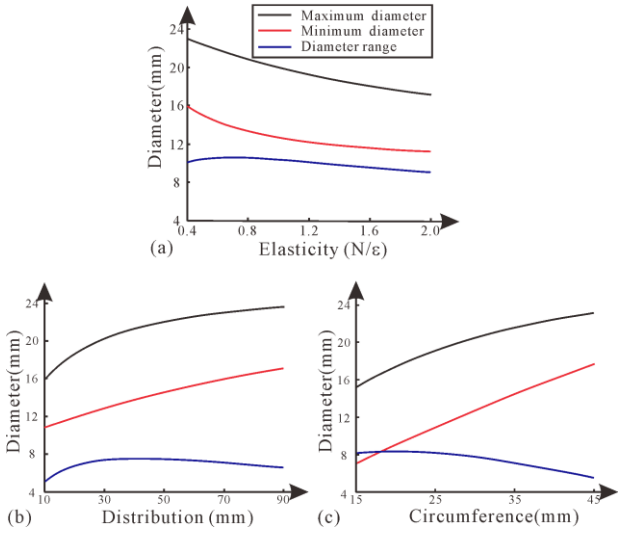

Figure 8. Effects of (a) the elasticity, (b) the distribution and (c) the circumference of the rubber band on the diameter range

the bands can still provide compression to a slim tube because of the comparingly larger strain. Therefore, the minimal diameter decreases more obviously, leading to a larger diameter range.

B. Response Time

The force versus time curve is presented in Fig. 9. It can be seen that the force increases linearly until the tube is heated. As for the constant loading speed, the linear stage shows a constant force increment rate. When the tube is heated, the force drops greatly for the disturbance, and then increases sharply. There are two reasons for the sharp increase. One is the increase of the Young's modulus of the fibers, contributing a larger overall stiffness. The other is the deployment of the tube. When the sensor compresses the tube, the tube is also deploying to the sensor, leading to a larger compression. However, when the phase change and deformation are completed, the whole system is stable, and the curve returns to be a linear configuration. The time it takes the system to return stable is regarded as the response time, which is 20s in this case.

C. Discussions

According to the Natural Orifice Surgery Consortium for Assessment and Research (NOSCAR) working group, it is very ideal for a manipulator to be compact in size and have a diameter of 20mm or less [8] considering the body orifice size. Tab. III compares the diameter of the existing surgical manipulators and platforms in NOTES, whose diameters vary from 18-22mm. With the proposed design method, the physical model can achieve a diameter range of 14.7-21.4mm. Its diameter ratio is 1.46, which can be easily improved to 1.6 at an optimized rubber band configuration, as shown in Fig. 8. Thus, if the braided skeleton exhibits a diameter of 20mm at deployment state, it is likely be folded to a profile of 20/1.6=12.5mm. It is similar to those of the commercial endoscopes at a range of 12.8-13.3mm [27], making the insertion process much smoother.

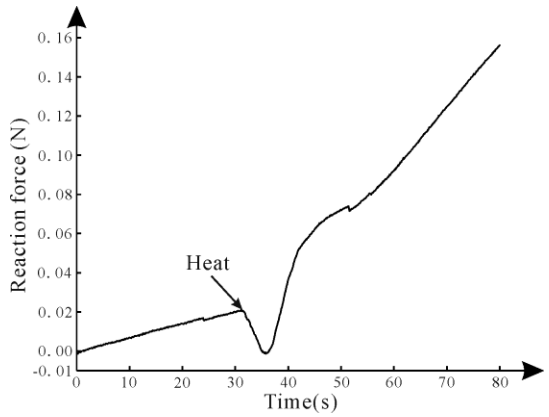

Figure 9. Response time determination: force versus time curve under tip load

TABLE III. OUTER DIAMETER OF THE EXISTING DEVICES

Manipulators/Platforms	Outer Diameter
Layer Jamming [12]	22.0mm
Dragon Skin [13]	20.0mm
DDES [25]	22.0mm
IOP [26]	18.0mm

Because of the heat actuation method, it will take about 20s to deploy the braided skeleton to a large-profile state. In the test of response time, it is heated from the room temperature. If a careful preheating is applied first, increasing the temperature slightly below the transition temperature, the deployment process will be greatly accelerated. As the braided skeleton should get coupled with the tunable stiffness mechanism and form the final manipulator, it can stiffen at vacuum to lock its large profile. In this way, the skeleton doesn't need to be charged during the surgery, which thus has enough time to cool down. It can still work properly without an active cooling element and return to slim state when the vacuum is stopped after the surgery.

Some practical problems should be considered to make the manipulator applicable. First is the large amount of heat caused by the current, which is not tolerable to the human body. Thus, a cover with great heat insulation should be designed. Next, a temperature monitor system may also help to avoid overheating and guarantee a suitable preheating. Then, how to deploy the manipulator at a bent configuration is another challenge. Finally, the heating system for tunable diameter and the vacuum system for tunable stiffness have to get coupled, making sealing a challenge in fabrication.

VI. CONCLUSION

In this paper, we propose a method based on nitinol fiber and rubber band to achieve tunable diameter of the braided tube in two directions, which can be used as the skeleton of the deployable surgical manipulator in NOTES. The experiment conducted validates the method, which achieves a tunable diameter range of 14.7mm to 21.4mm. In addition, a theoretical model is established, which analyzes the effects of rubber ring on the tunable diameter. The tube can achieve a diameter ratio of 1.6 at an optimized parameter group. The response time is also analyzed experimentally. It shows that 20s is needed to activate the tube. In the future, we will focus

on the integration of the tunable diameter and tunable stiffness mechanisms and fabrication of the final manipulator.

ACKNOWLEDGMENT

This work was supported by the National Key R&D Program of China (Grant No. 2017YFC0110401) and the National Natural Science Foundation of China (Grant 51520105006 and Grant 51721003).

REFERENCES

[1] T. H. Baron, "Natural orifice transluminal endoscopic surgery," Brit. J. Surg., vol. 94, no. 1, pp. 1-2, Jan. 2007.

[2] G. Stiff, M. Rhodes, A. Kelly, K. Telford, C. P. Armstrong, and B. I. Rees, "Long-term pain: Less common after laparoscopic than open cholecystectomy," Brit. J. Surg., vol. 81, no. 9, pp. 1368-1370, Sep. 1994.

[3] R. Tacchino, F. Greco, and D. Matera, "Single-incision laparoscopic cholecystectomy: Surgery without a visible scar," Surg. Endosc., vol. 23, no. 4, pp. 896-899, Apr. 2009.

[4] C. Zornig, H. Mofid, A. Emmermann, M. Alm, H. A. von Waldenfels, and C. Felixmuller, "Scarless cholecystectomy with combined transvaginal and transumbilical approach in a series of 20 patients," Surg. Endosc., vol. 22, no. 6, pp. 1427-1429, June 2008.

[5] J. Hochberger, and W. Lamade, "Transgastric surgery in the abdomen: the dawn of a new era?, " Gastrointest. Endosc., vol. 62, no. 2, pp. 293-296, Aug. 2005.

[6] D. Rattner, and A. Kalloo, "ASGE/SAGES working group on natural orifice translumenal endoscopic surgery," Surg. Endosc., vol. 20, no. 2, pp. 329-333, Feb. 2006.

[7] J. Bingener, and C. J. Gostout, "Update on natural orifice translumenal endoscopic surgery," Gastroenterol. Hepatol., vol. 8, no. 6, pp. 384-389, June 2012.

[8] National Orifice Surgery Consortium for Assessment and Research (NOSCARTM), "Working Group Summary on Development of A Multitasking platform," Available from: http://www.noscar.org/presentations-2006/tasking-platform, Oct. 2006.

[9] M. W. Gifari, H. Naghibi, S. Stramigioli, and M. Abayazid, "A review on recent advances in soft surgical robots for endoscopic applications," Int. J. Med. Robot. Comp., vol. 15, no. 5, p. e2020, Oct. 2019.

[10] S. Zuo, and S. Wang, "Current and emerging robotic assisted intervention for Notes," Expert Rev. Med. Devic., vol. 13, no. 12, pp. 1095-1105, Dec. 2016.

[11] Z. Shang, J. Ma, Z. You, and S. Wang, "A foldable manipulator with tunable stiffness based on braided structure," J. Biomed. Mater. Res. B, vol. 108, no. 2, pp. 316-325, Feb. 2020.

[12] Y. J. Kim, S. Cheng, S. Kim, and K. Iagnemma, "A novel layer jamming mechanism with tunable stiffness capability for minimally invasive surgery," IEEE Trans. Robot., vol. 29, no. 4, pp. 1031-1042, Aug. 2013.

[13] S. Zuo, K. Iijima, T. Tokumiya, and K. Masamune, "Variable stiffness outer sheath with 'Dragon skin' structure and negative pneumatic shape-locking mechanism," Int. J. Comput. Ass. Rad., vol. 9, no. 5, pp. 857-865, Sep. 2014.

[14] A. Yagi, K. Matsumiya, K. Masamune, H. Liao and T. Dohi, "Rigidflexible outer sheath model using slider linkage locking mechanism and air pressure for endoscopic surgery," in Proc. Int. Conf. Med. Image Comput. Comput.-Assisted Intervention (MICCAI), Copenhagen, Denmark, 2006, pp. 503–510.

[15] I. Falco, M. Cianchetti and A. Menciassi, "STIFF-FLOP surgical manipulator: design and preliminary motion evaluation," in Proc. 4th Workshop Computer/Robot Assisted Surgery (CRAS), Genoa, Italy, 2014, pp. 131-134.

[16] R. Wang, and K. Ravi-Chandar, "Mechanical response of a metallic aortic stent—Part I: pressure-diameter relationship," J. Appl. Mech., vol. 71, no. 5, pp. 697-705, Sep. 2004.

[17] M. De Beule, S. Van Cauter, P. Mortier, D. Van Loo, R. Van Impe, P. Verdonck, and B. Verhegghe, "Virtual optimization of self-expandable braided wire stents," Med. Eng. Phys., vol. 31, no. 4, pp. 448-453, May 2009.

[18] M. Schillinger, S. Sabeti, C. Loewe, P. Dick, J. Amighi, W. Mlekusch, O. Schlager, M. Cejna, J. Lammer, and E. Minar, "Balloon angioplasty versus implantation of nitinol stents in the superficial femoral artery," N. Engl. J. Med., vol. 354, no. 18, pp. 1879-1888, May 2006.

[19] P. Zamiri, Y. Kuang, U. Sharma, T. F. Ng, R. H. Busold, A. P. Rago, L. A. Core, and M. Palasis, "The biocompatibility of rapidly degrading polymeric stents in porcine carotid arteries," Biomaterials, vol. 31, no. 31, pp. 7847-7855, Nov. 2010.

[20] C. Singh, C. S. Wong, and X. Wang, "Medical textiles as vascular implants and their success to mimic natural arteries," J. Funct. Biomater., vol. 6, no. 3, pp. 500-525, Sep. 2015.

[21] D. Ma, G. F. Dargush, S. K. Natarajan, E. I. Levy, A. H. Siddiqui, and H. Meng, "Computer modeling of deployment and mechanical expansion of neurovascular flow diverter in patient-specific intracranial aneurysms," J. Biomech., vol. 45, no. 13, pp. 2256-2263, Aug. 2012.

[22] Z. Shang, S. Wang, Z. You and J. Ma, "A hybrid tubular braid with improved longitudinal stiffness for medical catheter," J. Mech. Med. Biol., vol. 19, no. 3, p. 1950003, May 2019.

[23] A. Rao, A. R. Srinivasa, and J. N. Reddy, Design of Shape Memory Alloy (SMA) Actuators. Berlin: Springer International Publishing, 2015, ch. 1.

[24] M. R. Jedwab, and C. O. Clerc, "A study of the geometrical and mechanical properties of a self-expanding metallic stent--theory and experiment," J. Appl. Biom., vol. 4, no. 1, pp. 77-85, Spr. 1993.

[25] C. C. Thompson, M. Ryo, N. J. Soper, E. S. Hungess, R. I. Rothstein, and L. L. Swanstrom, "Evaluation of a manually driven, multitasking platform for complex endoluminal and natural orifice transluminal endoscopic surgery applications (with video)," Gastrointest. Endosc., vol. 70, no. 1, pp. 121-125, Jul. 2009.

[26] L. L. Swanstrom, M. Whiteford, and Y. Khajanchee, "Developing essential tools to enable transgastric surgery," Surg. Endosc., vol. 22, no. 3, pp. 600-604, Mar. 2008.

[27] D. Hellier, F. Albermani, B. Evans, H. de Visser, C. Adam, and J. Passenger, "Flexural and torsional rigidity of colonoscopes at room and body temperatures," P. I. Mech. Eng. H, vol. 225, no. 4, pp. 389-399, Apr. 2011.